ZIBELINE INTERNATIONAL™ PUBLISHING

Acta Chemica Malaysia (ACMY)

DOI: http://doi.org/10.26480/acmy.02.2022.75.84

ISSN: 2576-6724 (Print)
ISSN: 2576-6732 (Online)
CODEN: ACMCCG

RESEARCH ARTICLE

EQUILIBRIUM, KINETIC AND MASS TRANSFER OPTIMIZATION STUDIES OF CATIONIC DYE ADSORPTION ONTO CHEMICALLY MODIFIED BIO-SORBENT DERIVED FROM LIGNOCELLULOSIC WASTE

Nworie, F. S[a], Ike-Amadi, A.C[b], Agha-Akpu J[a], Nworu, J[c]

[a]Department of Industrial Chemistry,Ebonyi State University, Abakaliki, Ebonyi State, Nigeria.
[b] Department of Chemistry, Abia State polytechnic, Abia State, Nigeria
[c] Department of Chemistry, Nigeria Maritime University, Okerenkoko, Delta State, Nigeria
****Corresponding Author Email: nworie.sunday@ebsu.edu.ng***

ARTICLE DETAILS

Article History:

Received 16 February 2022
Accepted 20 March 2022
Available online 23 March 2022

ABSTRACT

A one, two and three parametric equilibrium models as well as kinetic and mass transfer models were used to optimize the adsorption of cationic dye (methylene blue) onto a chemically modified biosorbent derived from plantain peels (PP) waste. The chemically modified PP was characterized using Braunauer-Emmett-Teller (BET), X-ray Diffraction (XRD), Fourier Transform Infra-red Spectroscopy (FTIR) and Scanning Electron Microscope (SEM). Parameters influencing adsorption were optimized and result indicated maximum adsorption at contact time of 120 S, pH of 8 and initial methylene blue (MTB) concentration of 7.75 × 10^{-6} mg/L. The maximum adsorption capacity was evaluated to be 222mmolkg^{-1}. The data simulated into the equilibrium models based on error analysis and coefficient of non-determination indicated that the adsorption process followed mainly the Hill equilibrium isotherm model and perfectly fits the Elovic kinetics and mass transfer process as the rate determining step. The modified PP is recommended for the removal of cationic dyes in effluents and aqueous media.

KEYWORDS

methylene blue, adsorption, equilibrium and kinetic models, error analysis, biochar, modification.

1. INTRODUCTION

There are over hundreds of thousand varieties of synthesized dyes (organic and inorganic) for industrial applications (Halil et al., 2017; Mahmoodi et al., 2011). These dyes are generally classified as anionic, non-ionic and cationic dyes and are regularly explored by most chemical industries (pulp, paper, textile, leather, printing, food) for several applications (El-Sayed, 2011; Mahmodi et al., 2011). On routine basis, these industries generate several wastes (effluents) through the use of these dyes, which are released into open water bodies and poses threat to the environment (Nworie et al., 2019). These effluents (by-products of dye processing) are mutagenic, non-biodegradable, highly toxic and hazardous which could cause human scaling, itching of the body and human body irritation (Halil et al., 2017; Nworie et al., 2019; Farouq and Yousef, 2015).

Azo dye contributes to over 50% of several tons of commercial dyes manufactured annually (Nworie et al., 2019; Pushpa et al., 2015; You et al., 2016). The migration, utilization and manufacturing of azo dyes are in many ways eco-unfriendly. The structure of azo dyes which has complex aromatic ring are non-susceptible to biodegradation to most oxidizing agents, temperature and structural modification on light exposure (Nworie et al., 2019; Yang et al., 2016). Methylene Blue (MTB) is an organic azo dye. The existence of MTB in wastewater (effluent) poses threat to the aquatic organisms in the water. Methylene blue can reduce the penetration ability of sunlight into the water body causing failure in the functions of the organs of the aquatic organisms (Halil et al., 2017; El-Sayed, 2011; Nworie et al., 2019; Yang et al., 2016). The increased level of bioaccumulation of organic dyes in wastewater is as a result of their resistance to temperature, degradation and structural modification.

Recently, the interest of industrial workers and researchers have been on the rise on possible ways to combat the hazardous and chromogenic effects associated with industrial effluents originating from azo dyes (Nworie et al., 2019; Yang et al., 2016; Kamal, 2009; Tan et al., 2008; Akkaya and Guzel, 2014; Santos et al., 2013). Flocculation, chemical coagulation, ozonation, membrane-based separation process, oxidation, biological process, photocatalytic process, electrochemical process, son chemical process and adsorption method are different methods that have been explored by industrial workers and researchers in decontamination of aqueous media containing dyes (Nworie et al., 2019; Pushpha et al., 2015; You et al., 2016; Akkaya and Guzel, 2014; Shakoor and Nasar, 2016; Pereira et al., 2009; Etim et al., 2016; Coskun et al., 2017; Ozdes et al., 2010). Among the methods, adsorption process stands out to be the most effective, efficient and environmentally friendly process (Nworie et al., 2009; Yang et al., 2016; Kamal, 2009). Also, the use of activated carbon in the adsorption process yields greater result, but the increased cost of activated carbon poses lots of limitations to researchers which have led to the search for alternative materials with cost efficiency and environmental safety (Nworie et al., 2019; Kamal, 2009; Mazhar et al., 2014; Nworie et al., 2020; Komkiene and Baltrenaite, 2016; Inyang et al., 2011; Okareh and Adeolu, 2015; Onyebado et al., 2004; Betiku and Sheriff, 2014).

Quick Response Code	Access this article online	
	Website: www.actachemicamalaysia.com	**DOI:** 10.26480/acmy.02.2022.75.84

Cite the Article: Nworie, F. S, Ike-Amadi, A.C, Agha-Akpu J, Nworu, J (2022). Equilibrium, Kinetic and Mass Transfer Optimization Studies of Cationic Dye Adsorption Onto Chemically Modified Bio-Sorbent Derived from Lignocellulosic Waste. *Acta Chemica Malaysia, 6(2): 75-84.*

Plantain wastes are indiscriminately disposed to the environment due to their less human application and they contribute to the environmental hazards by clogging the water ways and contributing to the foul-smelling nature of the environment (Tiwari and Lee, 2012; Nworie, 2018). Plantain peel biochar (PPB) a solid component of the thermal degradation (carbonization or pyrolysis) of plantain wastes gives an eco-friendly biomaterial capable of decongesting metal polluted sites as well as effluents ridden with anionic or cationic dyes (Nworie, 2018). Characteristically, biochar is environmentally benign, with high surface area, modifiable, scalable and fine-tuneable. Acid, basic, chelating agent modified biochar have been used for the sorption of heavy metals, organic and inorganic contaminants from samples with promising results due to increased functionality and mechanical stability.

To combat the risks posed by the industrial indiscriminate disposal of MTB, plantain peel was converted into an activated biochar, modified with nitric acid and used as an effective, economical and eco-friendly adsorbent which has increased adsorptive capacity, high surface area and increased surface activity with high capability of decontaminating aqueous media with environmental toxicants such as drinking water, wastewater and other industrial effluents (Nworie et al., 2019). The equilibrium and kinetic studies were carried out for the interpretation of the adsorption process involving mass transfer and surface interaction. The adsorption models and kinetic models were used for the optimization of the industrial design while the chemical characterization using FTIR, SEM, XRD and BET ensures structural and surface characterization of the biosorbent for adsorption efficiency.

2. Material and Methods

2.1 Materials

Analytical grade reagents H_2SO_4, HNO_3, NaOH, HCl, were all obtained from Sigma Aldrich® and used without further purification unless indicated. The MTB (3,7-bis(dimethylamino)-phenazathionium tetramethylthionine chloride) with molecular weight and molecular formular of 373.9 g/mol $C_{16}H_{18}N_3SCl.3H_2O$ respectively is shown in Figure 1. The stock solution of MTB (100 mg dm^{-3}) was prepared in pH solution of 7. Double distilled water was used for all experiments.

2.2 Characterization of the Modified Plantain Peel Biochar (MPPB)

The BET surface area and pore size of MPPB was measured using Micromeritics ASAP 2020 system. X-ray diffraction pattern was obtained on a Bruker® D8 Discover diffractometer, equipped with a Lynx Eye detector, under Cu-Ka radiation (l ¼ 1.5405 Å) and data collected in the range of 2θ =10 to 100°, scanning rate at 0.010omin^{-1},192 s per step and samples placed on a zero-background silicon wafer slide. Cary 630 Agilent Technologies, USA was used for functional group determination (FTIR). The concentration of the unabsorbed MTB in solution after equilibration was evaluated spectrophotometrically at wavelength of 670 nm using Jenway UV – Vis spectrophotometer model 6105 after centrifuge with Gulfex medical scientific England centrifuge model 800D. The structure and morphology (SEM) of MPPB was determined using Phenomprox by Phenom world Eindhoven, Netherlands. The ash, protein and nitrogen part of PP were determined using Kjeldahl method whereas the lignin and cellulose part were evaluated as reported in another study (Nworie, 2018).

2.3 Sample Collection and Preparation

The waste plantain peels *(Musa paradisiaca)* was collected from Abakaliki metropolis in Ebonyi state of Nigeria in distilled water washed plastic containers. The waste PP were cleaned, sun dried for 7 days and consequently oven dried at 60°C for 24 h. The modified method was adopted for carbonization of the dried PP (Tiwari and Lee, 2012). This was achieved at a temperature of 600°C in nitrogen environment in a muffle furnace for 6 h. The resulting biochar was cooled at room temperature, ground to fine powder, and then modified. A portion of 10 g of the carbonized PP was transferred into a 500 mL container and 30 mL of concentrated HNO_3 added with continuous stirring for 2 h. The mixture was diluted with deionized water and decanted several times and then washed with double distilled water until the pH was tested to be 6.8. The product formed regarded as modified plantain peel biochar (MPPB) was then dried in an oven at a temperature of 110°C.

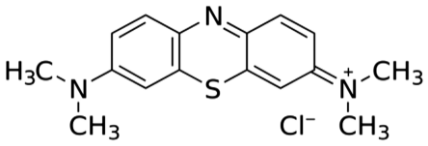

Figure 1: Structure of MTB.

2.4 Batch Sorption Studies

The batch extraction studies were applied to study the sorption of MTB onto MPPB. To determine the effect of initial MTB concentration in the sorption process, 0.5 g of MPPB was transferred into four separate 250 cm^3conical flasks containing 10 cm^3MTB solution of varied concentrations (3.1-7.75 ×10^{-6}mg dm^{-3}) maintained at pH of 6.8. The mechanical shaker (Remi equipment) operating at 150 rpm and 303 K was used to equilibrate the mixture for 120 min for equilibrium to be achieved. The time for maximum sorption was evaluated by measuring 10 cm^3 of 7.75 ×10^{-6}mg dm^{-3}into four separate containers with 0.5 g of MPPB added to each with time varied between 30-150 Min. The containers were equilibrated mechanically and removed at time intervals of 30, 60, 90, 120 and 150 min and concentration of MTB unadsorbed determined spectrophotometrically after filtration with what man filter paper No 1 and centrifugation at 5000 rpm for 4 min. To evaluate the effect of pH on the sorption of MTB on MPPB, the pH was varied from 1 to 10. In the process, 0.5 g of the MPPB was transferred into a series of containers with 10 $cm^3$of 7.75 ×10^{-6}mg dm^{-3}MTB each. The mixture was treated as described under initial MTB concentration.

To evaluate the quantity of MTB adsorbed at equilibrium qe(mg/g), equation 1 was applied, the percentage MTB (%) removed using MPPB was evaluated using equation 2 while the amount of MTB sorbed at a given time t by MPPB (qt,(mg/g)) was determined using equation 3.

$$q_e = \frac{(Co - Ce)V}{M} \quad (1)$$

$$\%\ \text{MTB Sorbed} = \frac{Co - Ce}{Co} \times 100 \quad (2)$$

$$q_t = \frac{(Co - Ct)V}{M} \quad (3)$$

Here, Co(mg/L), Ce (mg/L),Ct (mg/g),V(L) and M (g) stands for the initial MTB concentration, concentration of MTB at equilibrium, concentration of MTB at time t, volume of solution and weight of MPPB respectively.

2.5 Point of Zero Charge Determination (pH_{zpc})

The point of zero charge which typifies the dependence of MPPB on the charge and surface functionalities of the sorption process was evaluated as described in another study with slight pH modification using 0.1 M HCl/NH_3 instead of 0.1 M HCl/NaOH solutions (Phansiri et al., 2015). The pH_{zpc} value of 6.8 was determined and applied in the study.

3. Results and Discussion

Determination of the proximate composition of MPPB was done using the Kjeldahl method as described elsewhere [4]. From the result obtained, MPPB contains high percentage of lignin and cellulose of 58.26 ± 0.285 %, ash content of 25.50± 0.250 %, protein content of 14.00± 0.360% and nitrogen content of 2.24± 0.048 %. The lignin and cellulosic composition of the polymer is 18.35% higher than the lignocellulosic content of activated rice husk biochar as reported elsewhere and 13.26 % higher than those of brewers spent grain (Nworie et al., 2019; Antonija et al., 2018).

3.1 Brunauer, Emmett, Teller (BET): Surface Area and Pore Size Analysis

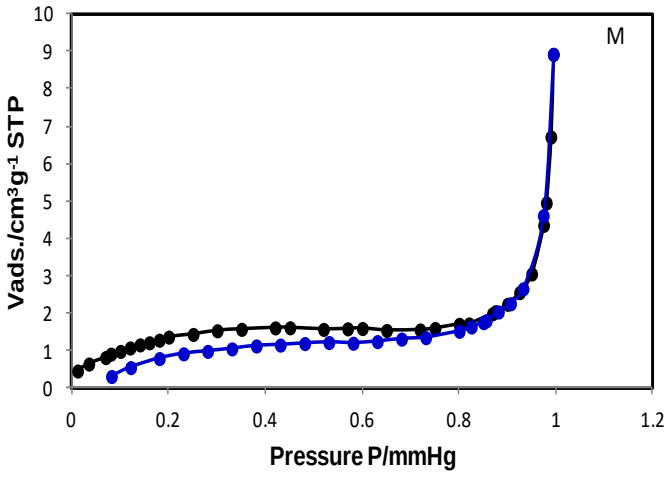

Figure 2: BET Surface Area of MPPB

The nitrogen adsorption/desorption isothermplot of MPPB showing the BET isotherm is shown in Figure 2. A vividlookat the isotherm indicated its mesoporous nature indicating the biosorbent as nanosized (Alothman, 2012). The shift in the STPg^{-1} for MPPB isotherm was observed to be 15 cm^3 with surface area and pore size as 8.79 m^2/gand 16.69 cc/g respectively. It could be observed from the BET analysis presented in Figure 2 thatthe large surface area per gram of a sample of the MPPBindicated greater propensity to capture and MTB being a nanobiorsorbent.

Figure 3 shows the XRD (Cu-Ka radiation) patterns of MPPB.From Figure 3, a sharp peak was seen at 2θ = 40.53°followed withcertain specie degradationin biochar formation at 2θ = 24.24 and 31.31°(30). As shown in Equation 1, there was observable ordered crystallinity of the biosorbent and Scherrer Equation (Equation 1) was used to evaluateaverage crystallite size (nm) as 14.56 nm a further confirmation of the mesoporosity of MPPB as nanosized (Nworie et al., 2019; Jianjian et al., 2018).

$$d = \frac{K\lambda}{\beta Cos\theta} \quad (4)$$

K, β, λ and θ represents Scherer constant, full width at half maximum, wavelength and Bragg angle respectively.

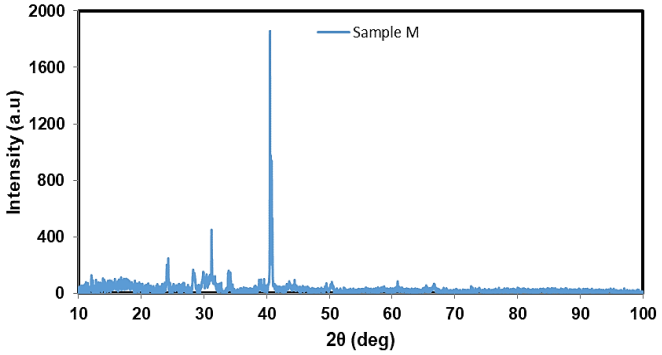

Figure 3: X-ray diffractogram of MPPB.

3.2 FTIR Analysis of MPPB

The functional groups present in MPPB was determined using FTIR. From the result shown in Figure 4, a broad band which shows hydroxyl group(-OH) was seen at 3421 cm^{-1}due to O-H stretching vibration of intra and intermolecular hydrogen bonding (Banerjee and Chattopadyaya, 2017; Kezerle et al., 2018). Bands observed at 2855 and 2922 cm^{-1}could be due to the presence of $-CH_2$ groups (Zhang et al., 2019). The carbonyl group(C=O) band and C=C phenol ring stretching vibration were seen at 1744 $cm^{-1}$and 1461 cm^{-1} respectively (Kezerle et al., 2018; Nworie et al., 2020). At 1371 cm^{-1}a band was observed and could be due to C-N stretching amine group (Nworie et al., 2019). Between 857 to 763 cm^{-1}, the band seen could be due to ester vibration of monosubstituted aromatic rings (Kezerle et al., 2018; Nworie et al., 2018).

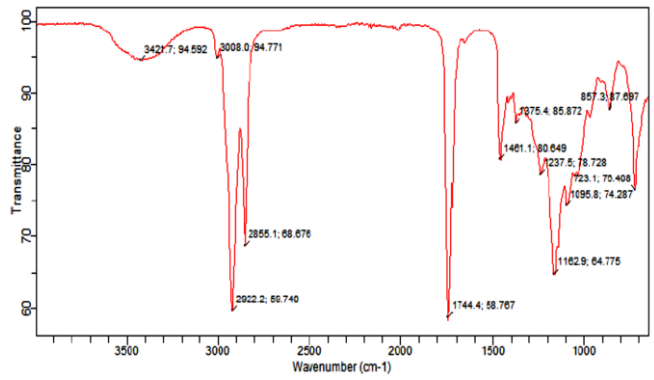

Figure 4: FTIR spectra of MPPB

3.3 SEM Analysis of MPPB

The structure and morphology of MPPB as determined using SEM is shown in Figure 5. The SEM imageindicated irregular porous surface. The structure is consistent with other lignocellulosic biomaterials derived from plantain peels and banana wastes (Nworie et al., 2020). The irregular porous morphologyindicated an excellent multifunctional surface for efficient capturing of sorbates.

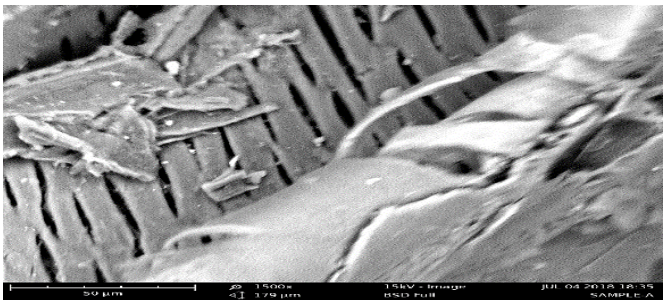

Figure 5: SEM Micrographs of MPPB

3.4 pH Influence on MTB Removal from Aqueous Solution

The contaminant removal potency of every sorbent is highly influenced by the pH (Nworie et al., 2019). The sorbent characteristics to a great extent influences the sorption capacity and such properties such as surface functionalities, mechanical stability, surface charge and degree of solution sorbate ionization. In other to evaluate the influence of pH on the sorption capacity of MTB onto MPPB, the pH was varied between 1-10 at 303 K for 120 min and the observed result indicated in Figure 6. The maximum MTB sorbed was 0.1528 × 10^{-6}mg/g at pH 8 and the minimum observed was0.117 × 10^{-6} mg/g at pH 1. The removal of MTB between pH 9-10 was almost at constant and the observation is consistent with other studies on the sorption of cationic dyes using biomaterials (Nworie et al., 2019). The low values of MTB removed at acidic pH zones as against basic pH zones which are higher could be attributed to the reduced electrostatic forces of attraction between cationic MTB surfaces and positively charged MPPB (You et al., 2016; Nworie and Spectural, 2018).

Therefore, due to similar charges on the surface of MTB and MPPB adsorption was greatly reduced as a consequence of competition (Nworie and Spectural, 2018). Increase in pH from 6 and above led to increase in negative sites and charges on MPPB and an increase in adsorption. This could be as a result of increased electrostatic attraction due to the presence of –OH at the basic region. Alteration in sorption could be basically due to multifunctional dissociation processes on the surface of MPPB causing a shift in the equilibrium (Mahmoodi et al., 2011). The favourable sorption of a contaminant is greatly determined by the point of zero charge which in this case was determined to be 6.8. If a solution pH is greater than pH_{zpc} there will be cationic attraction as MPPB is of negatively charged surface. However, if the solution pH is lower than $pH_{zpc,}$ there will be anionic attraction on the positive charge of MPPB (Nworie et al., 2019).

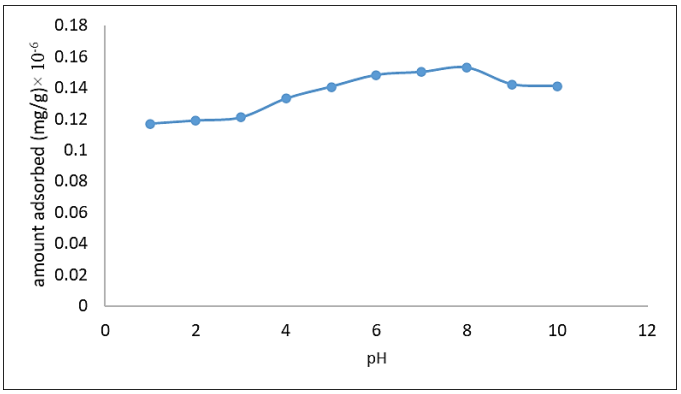

Figure 6: Effect of pH on the adsorption of MTB at 303 K and 120 min.

3.5 Effect of Initial MTB Concentration on the Removal efficiency

The effect of initial MTB concentration on the sorption was studied by varying the concentration of MTB between 3.1 to 7.75×10^{-6} mg/L and the result shown in Figure 7. Based on the plot and in compliance with other studies, the amount of MTB adsorbed increased linearly as the concentration increased (Phansiri et al., 2015; Nworie et al., 2019). The adsorption capacity was observed to increase from 2.0 × 10^{-6} to 8.0 × 10^{-6} mg/g as equilibrium was attained an indication of increased fractional sorption of MTB in the adsorption process. The sorption of MTB increased linearly from 2.96 × 10^{-6} to 7.55 × 10^{-6} mg/L but above7.55 × 10^{-6} mg/L, there was observed regress in the sorption capacity as equilibrium was reached. The sorption of MTB into the empty exposed surfaces of MPPB is evidently observed to be controlled by Elovic, mass transfer and Weber and Moris intra-particle diffusion mechanisms from the kinetic and mass transfer model studies.

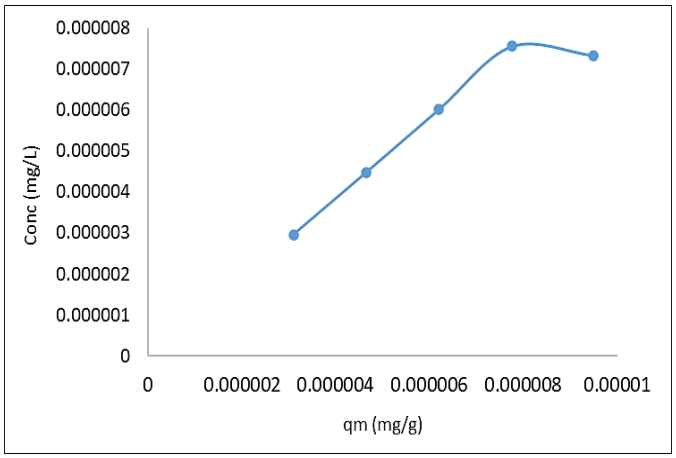

Figure 7: Effect of initial MTB concentration on the adsorption of MTB at 303 K and 120 min

3.6 Effect of Time of Contact on the Sorption of MTB

The effect of time of contact forthe sorption of MTB onto MPPB was executed by variation of time between 30-150 min at 303K for initial MTB concentration of 7.55 × 10^{-6} and result shown in Figure 8. From Figure 8, it could be shown that the sorption of MTB onto MPPB increased as time increased from 30 to 120 min where equilibrium was attained. The sorption capacity increased from 0.023 to 0.095 × 10^{-6} mg/g for time increase from 30 to 120 mins above which a regress in adsorption was noticed. Actually, at the onset, the multifunctional surfaces of MPPB was exposed and rapid sorption of MTB was observed which rather decreased as the pores of MPPB got filled up and a consequent decrease in sorption. This observation is consistent with other works on the use of modified biochar for the removal of cationic dyes from aqueous solutions (Nworie et al., 2019; Etim et al., 2016; Betiku and Sheriff, 2014; Phansiri et al., 2015).

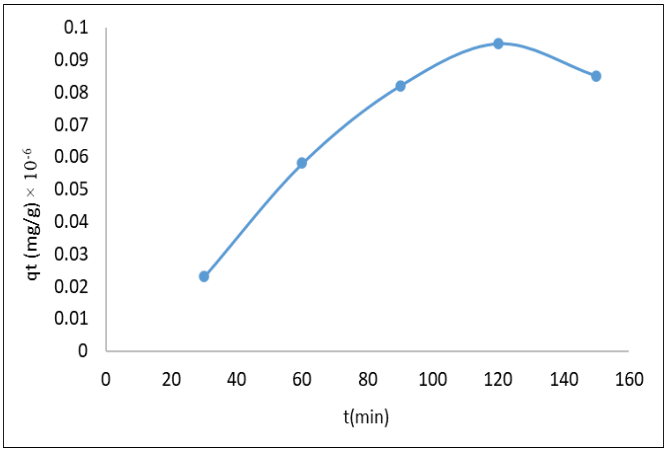

Figure 8: Effect of time of contact on the adsorption of MTB at 303 K and 120 min.

3.7 Adsorption Equilibrium

A study to gauge the distribution of MTB between the sorbent and sorbate at equilibrium of sorption was undertaken to determine the efficiency and applicability of MPPB using Henry, Elovic, Langmuir, Jovanovic, Harkin-Jura, Freundlich, Hill, Temkin and Redlich Peterson models.

3.8 Henry Sorption Model

A one parametric Henry model rarely studied was used to evaluate the fitness and applicability of the sorption data. The linear plot of the model represented in Figure 9 stems from the assumption of negligence to surface coverage and low adsorbate concentration (Nworie et al., 2019). The plot of qe versus Ce as shown in Figure 9 with linearized equation in Table 1 and values in Table 3 shows that the correlation coefficient (R2) is 0.9126, coefficient of non-determination (CND) as 0.0874. Henrys adsorption constant (KHE) from Figure 9 was observed to be 87.64. In comparison to other models, Henrys model could not perfectly simulate the data. Similarly, surface coverage is also a key factor in the sorption since Weber and Moris intra-particle diffusion process is kinetically part of the process that controls the mechanism.

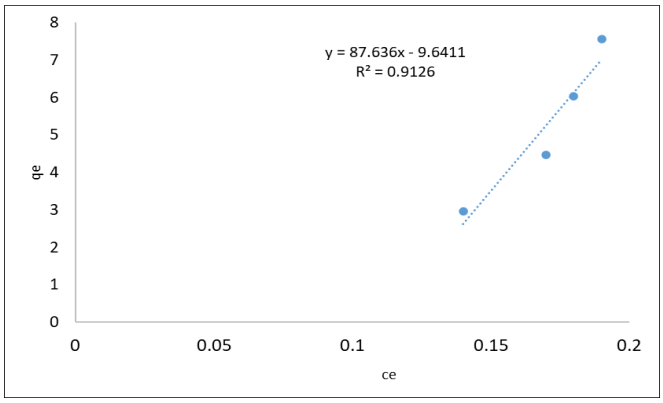

Figure 9: Henrys adsorption isotherm for the sorption of MTB onto MPPB at 303 K and 120 min

3.9 Langmuir Sorption Model

The linearized form of Langmuir model is presented in Table 1 with model constants in Table 3. The plot of Ce/qe versus Ce represented in Figure 10 which deduces whether the sorption follows a monolayer coverage with homogeneous sorbent sites consequent upon transmigration (Phansiri et al., 2015; Nworie et al., 2019). From Figure 10, $R^2$was 0.9836 with qm, the Langmuir constant as 222 $mmolkg^{-1}$ which compares favourably with those of other commercial activated carbons and biosynthetic sorbents (101-395 $mmolkg^{-}$) and (11-680 $mmolkg^{-}$) respectively (Nworie et al., 2019; Zhang et al., 2019). The Langmuir model equation (Equation 4) incorporates sorptionsites of fixed numbers with sorption reversibility (Halil et al., 2017; Phansiri et al., 2015).

$$q_{e=} \frac{q_m b C_e}{1+bC_e} \quad (4)$$

q_m, b, qe and Ce represents maximum sorption capacity of MPPB (mg/g), Langmuir constant related to free interaction binding energies of the adsorption (L/mg), amount of MTB sorbed per specific unit mass of MPPB (mg/g) and equilibrium concentration of MTB (mg/L) respectively.

Of high relevance in adsorption is the derivation of the dimensionless separation factor R_L which shows the desirability and favorability of the model. Hall equation (equation 5) was used to evaluateR_L and the value was favourable (0.343) according to the classificationof linear (R_L = 1), unfavorable (R_L> 1) and favorable (0 <R_L< 1).

$$\mathrm{RL} = \frac{1}{1+\mathrm{bXo}} \quad (5)$$

Xo represents initial concentration of MTB.

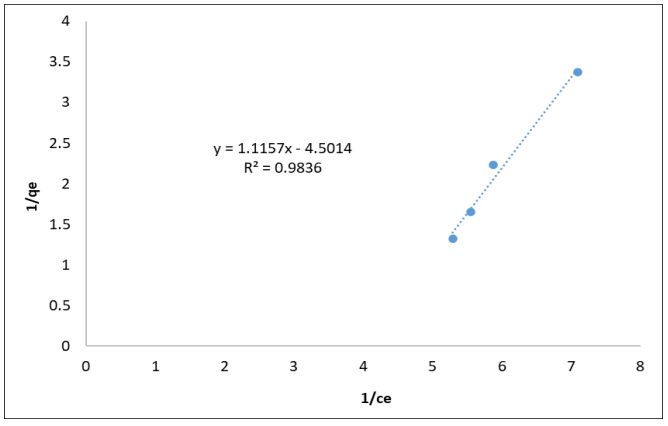

Figure 10: Langmuir isotherm model for the sorption of MTB onto MPPB at 303 K and 120 min.

3.10 Freundlich Isotherm

Data for the sorption of MTB onto MPPB was subjected to Freundlich sorption isotherm and the linear plot of Inqe versus In Ce shown in Figure 11. The Freundlich isotherm (equation 6) linear model is shown in Table 1 and illustrates sorption taking place in a heterogeneous, unlimited multilayer surface, with non-uniformly distributed energies (Phansiri et al., 2015; Nworie et al., 2020). As shown in Figure 11, simulating data into Freundlich isotherm gives R^2as 0.9388 with n the adsorption intensity which determines the adsorption favourability and gives the level of

deviation of the model from linearity as 0.0290and K_f value indicating the adsorption capacity as 8.135. The n value is less than unity, an indication that the process cannot simulate the MPPB –MTB interaction perfectly well (Phansiri et al., 2015; Mahmoodi et al., 2011).

$$qe = K_F Ce^{1/n} \quad (6)$$

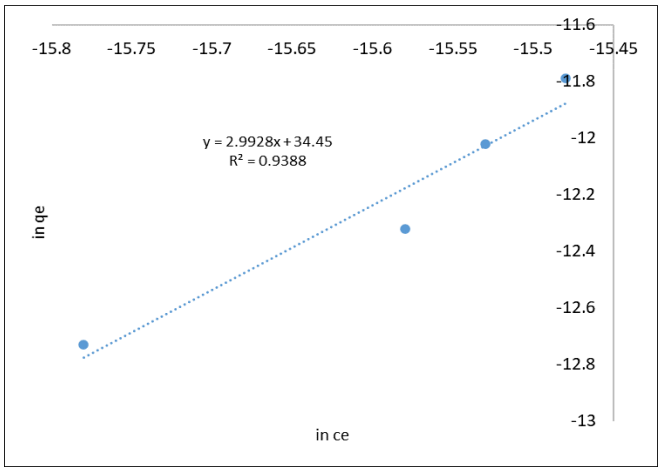

Figure 11: Freundlich isotherm for the sorption of MTB onto MPPB at 303 K and 120 min

3.11 Temkin Isotherm

The data was fitted into Temkins isotherm model to assess whether there is linear decrease of heat of adsorption with coverage sites under a co-operative condition. The model is presented in equation 7 with β and A representing heat of sorption and equilibrium binding constants respectively and the linearized form shown in Table 1.

$$q_e = \beta \mathrm{In} A_t + \beta InCe \quad (7)$$

The linear plot of q_e versus In C_e (Figure 12) generates a slope(A_T) and intercept (β) as 11.05 and 0.163 respectively with 0.8679 as values of R^2.The $R^2$is lowand cannot simulate the data perfectly well.

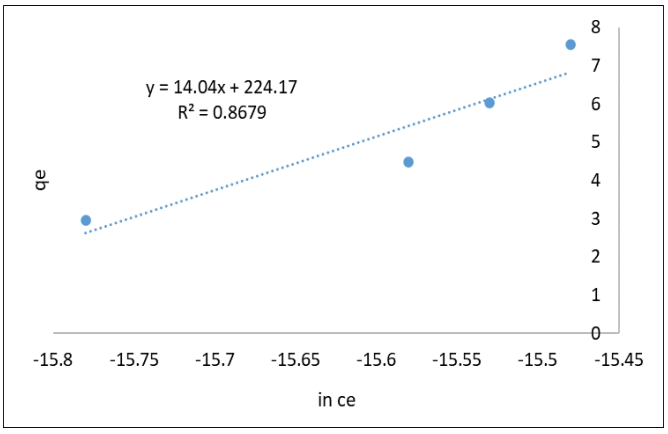

Figure 12: Temkin isotherm plot for the sorption of MEB onto ARHBat 303 K and 120 min

3.12 Elovic Isotherm Model

Elovic model describes sorption to proceed exponentially as sorption sites increases in a multilayer pattern. The sorption of MTB onto MPPB based on the high R^2 (0.9969) from plot of In (q_e/C_e) versus q_e (Figure 13)could be said to be multilayer at a glance but deeper consideration implicated lower adsorption capacity value disapproving the multilayer assumption (Table 3). On comparison with Hill isotherm which involves monolayer adsorption and with R^2 of 1, finally indicated that the sorption does not fit into Elovic model. The result observed is consistent with other studies involving cationic dye removal from samples using modified biosorbents (Nworie and Spectral, 2018). The Elovic isotherm model is shown in equation 8, the linear form in Table 1 with Km (slope) and K_E(intercept) as constants representing maximum adsorption capacity and adsorption constant respectively.

$$\frac{\mathrm{qe}}{\mathrm{qm}} = K_E Ce^{e^{\frac{qe}{qm}}} \quad (8)$$

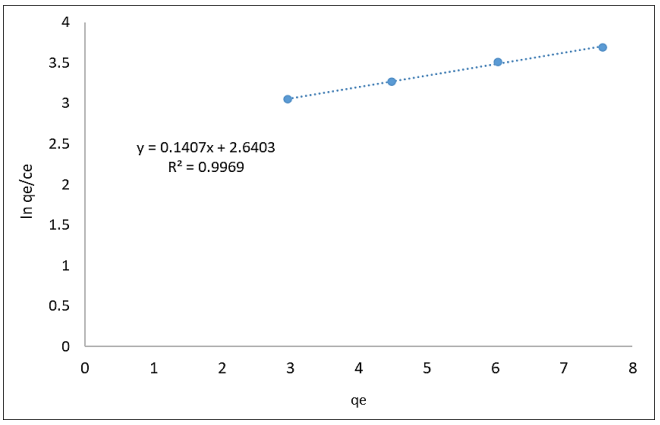

Figure 13: Elovic isotherm model plot for the sorption of MTB onto MPPBat 303 K and 120 min

3.13 Jovanovic Isotherm Model

To furtherstudy the applicability of the sorption models in the sorption process, Jovanovic isotherm model which incorporates mechanical interaction into Langmuir model was used. The model linearized form is shown in Table 1and the plot of Inq_e versus Ce (Figure 14) gives high R^2 (0.9682) which is lesser than that of Langmuir isotherm model (R^2 = 0.9836). The inability of the model R^2 value to overtake the Langmuir R^2value entails total absence of mechanical interaction and the observation is consistent with similar studies (Phansiri et al., 2015).

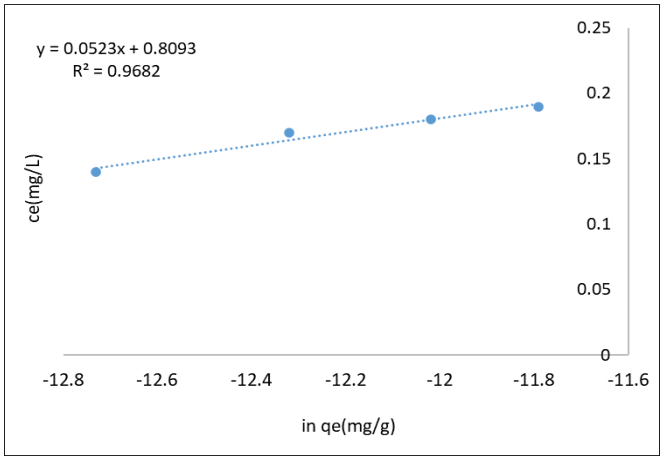

Figure 14: Jovanovic isotherm model plot for the sorption of MTB onto MPPBat 303 K and 120 min

3.14 Harkin-Jura Isotherm Model

The data from the sorption were also fitted into the Harkin-Jura isotherm model to determine the possibility of multilayer sorption arising from heterogeneous sorbate distribution on sorbent surface. The linear model form is presented in Table 1 with the linear plot of $1/qe^2$ versus log Ce in Figure 15. From the plot, R^2 value is 0.4738 which is very low to simulate the data efficiently well. The model gave the smallest R^2 value and highest coefficient of non-determination from the error analysis eliminating the possibility of multilayer adsorption as the best fit. This further supports the observation from Elovic model which eliminated multilayer sorption as a possibility in the adsorption process.

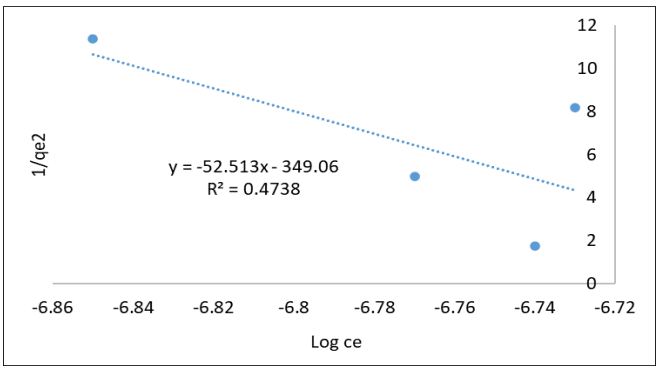

Figure 15: Harkin-Jura isotherm model plot for the sorption of MTB onto MPPB at 303 K and 120 min

3.15 Hill Isotherm model

The data from the sorption experiment was fitted into the Hill isotherm model to evaluate one of the three possibilities of separate homogeneous molecules ligating to surfaces as negative, non-co-operative or positive. Herein, MTB molecules could be studied as interacting with the MPPB surfaces in different binding sites (Nworie et al., 2019; Yang et al., 2016). The linearized model equation of Hill isotherm is illustrated in Table 1 and the plot of Log qe/1-qe against Log Co is shown in Figure 16. From the linear model and Figure 16, the constant $K_D$represents Hill dissociation constant and nH represents Hill coefficient for interaction which defines the molecular co-operativity. The nH value which was evaluated to be 2.51 illustrates the molecular co-operativity for the complexation of MTB onto MPPB as positive. The value of 2.51 is seen to be greater than unity with R^2 as 1. This shows a perfect fit and the model has the highest R^2 in comparison to other model isotherms.

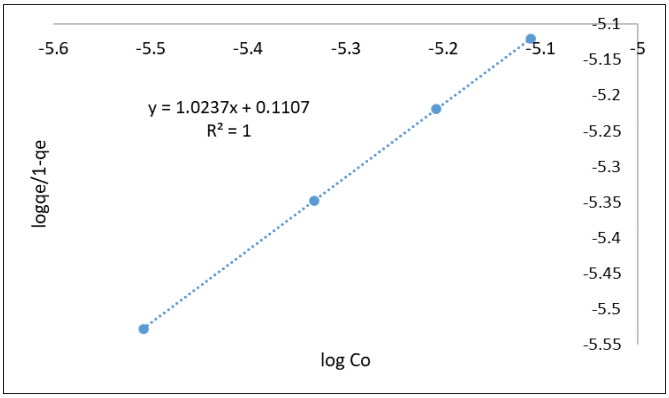

Figure 16: Hill isotherm model plot for the sorption of MEB onto ARHBat 303 K and 120 min

3.16 Redlich- Peterson Isotherm model

This is a three parametric equilibrium model isotherm which combines both Freundlich and Langmuir models with multilayer sorption in focus (Nworie et al., 2019). The linearized equation of the model is shown in Table 1 while the linear plot of In (Ce/qe) versus In Ce is illustrated in Figure 17. One of the Redlich-Peterson constants which is also regarded as absorptivity capacity constant is A (Lg^{-1}), the other parameters B (Lmg^{-1}) and β (mgL^{-1}) stands for a constant and (0 < β <1) representing an exponent respectively. When β =1 and β = 0 are two limiting conditions for the Langmuir and Freundlich isotherms respectively. Considering Table 3 and Figure 17 shows R^2 value of 0.8785 and β value of 0.99 almost unity. This further corroborates monolayer sorption before now confirmed using other models.

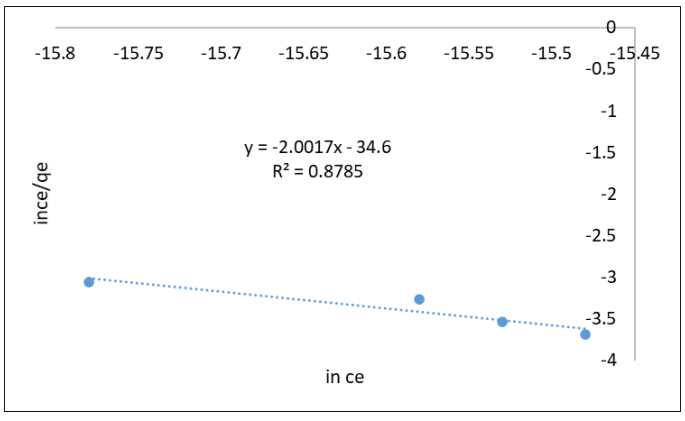

Figure 17: Redlich-Peterson isotherm model plot for the adsorption of MTB onto MPPBat 303 K and 120 min

3.17 Kinetic Models

3.17.1 Pseudo-first- order model

Equation 9 described the sorption of MTB onto MPPB as described using Lagergren pseudo-first- order rate where t, qt, qe and K_I represents contact time (min), qtis amount of MTB sorbed at time t, qe is amount of MTB sorbed at equilibrium (mg/g) and $K_1$the pseudo first order rate constant (Yang et al., 2016; Nworie and Spectral, 2018).

$$\log(qe - qt) = \log qe - (\frac{k_I}{2.303})t \quad (9)$$

From Figure 17and Table 4, the simulated data has high R^2 value of 0.9811 but very low K_1value 0.010 min^{-1}. The value of CND evaluated form 1-R^2 was though low (Table 4) but higher than those of Elovic and mass transfer model. Therefore, the higher value of R^2 value of Elovic kinetic model (0.9988) and mass transfer model (0.9986) indicates that the process is mainly controlled by chemisorption and not physisorption.

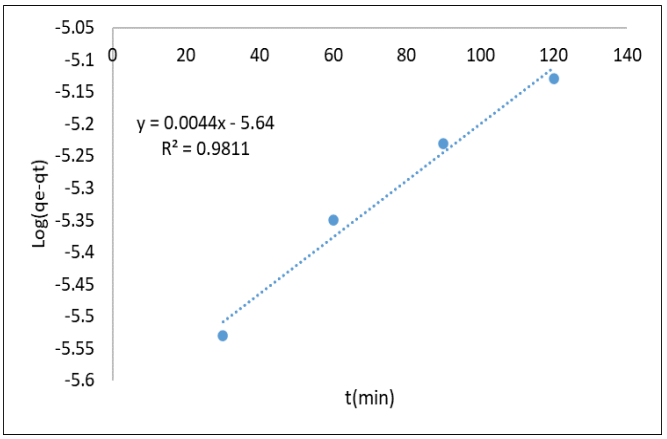

Figure 18: Pseudo-first –order kinetic plot for the adsorption of MTB onto MPPB at 303 K and 120 min

3.17.2 Pseudo-second-order kinetic model

Simulating the data obtained from the kinetic experiment into the pseudo-second-order kinetic model represented in equation 13 with focus on chemisorption in charge of the rate limiting step indicated R^2 value of 0.9597 (Figure 18) (Nworie et al., 2019).

$$t/qt = 1/K_2\, qe^2 + t/qe 13$$

From equation 13, t, K_2 and qe represents time of contact (min), second order rate constant (g/mg min) and adsorption capacity at equilibrium. The last two parameters are extracted from the intercept and slope of the linear plot of t/qt versus t (Figure 18). From Figure 18, the R^2 value is high, but lower than Elovic and mass transfer models. However, both Elovic and pseudo-second-order models support chemisorption as the rate limiting step.

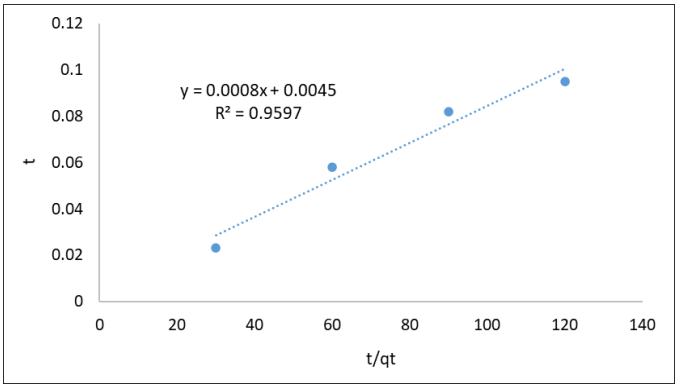

Figure 18: Pseudo -second –order kinetics plot for the adsorption of MTB onto MPPB at 303 K and 120 min

3.18 Elovic Kinetic Model

The kinetic data was further simulated into the Elovic kinetic model to further confirm the chemisorptive nature of the sorption of MTB onto MPPB. The Elovic kinetic model is shown in equation 14 with the constant α as Elovic constants for initial sorption rate ($mg/gmin^{-1}$) and β as magnitude of surface coverage and activation energy for chemisorption (g/mg) while the linear form is shown in Table 2 (Mazhar et al., 2014; Yang et al., 2016).

$$q_t = \frac{1}{\beta}\ln(\alpha\beta) + \frac{1}{\beta}In(t) \quad (10)$$

From Figure 19, R^2 value was highest (0.9988) indicating the process as to proceed by chemisorption with the linearized plot of q_t against In t showing the Elovic constants of α and β as -6.42 and 2.94 respectively.The high R^2 value suggested that diffusion and mass transfer process are part of the rate determining step and as shown by the R^2 values of Weber and

Morris intra-particle diffusion model and mass transfer mode (Table 4). Consequently, the involvement of diffusion in the sorption indicates absence of desorption or its occurrence at a negligible rate (Yang et al., 2016).

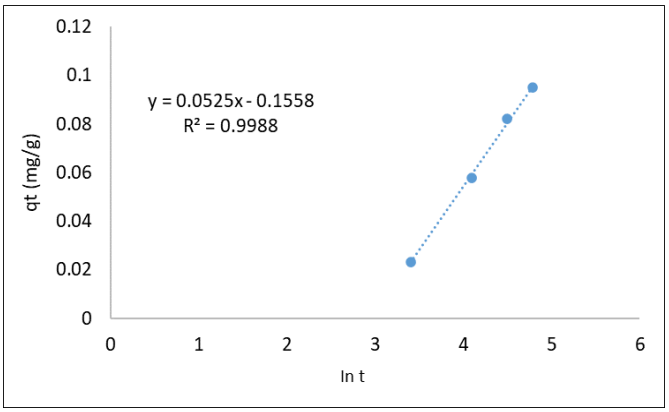

Figure 19: Elovic kinetic plot for the adsorption of MTB onto MPPBat 303 K and 120 min

3.19 Weber and Morris Intra-Particle Diffusion Model

To determine the intra-particle diffusivity of the sorption process, Weber and Morris intra-particle diffusion model was applied to the sorption process. The model equation (equation 15) with K_I (slope) which shows the intra-particle diffusion rate constant (mg/g $min^{1/2}$) and C (intercept) a constant related to the thickness of the boundary layer and the linearized form illustrated in Table 2 (Phansiri et al., 2015).

$$qt = K_I t^{1/2} + C \quad (11)$$

The linear plot of qt versus $t^{1/2}$ represented in Figure 20 has a high R^2 value of 0.9891. The value of C a measure of the magnitude of adsorption capacity was rather unexpectedly very low (Table 4) and therefore could not further justify the intra-particle diffusivity of the MTB through the surface of theMPPB. Further consideration of Figure 20 indicated the inability of the linear plot to pass through the origin. This is an indication that the intra-particle diffusion is part of the rate limiting step but not solely the only kinetic model in control of the sorption (Kamal, 2009). Therefore, existence of boundary layer control is implicated as the intercept line fails to proceed through the origin.

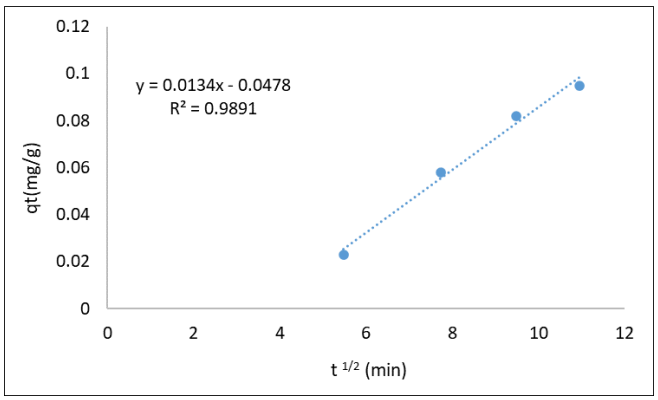

Figure 20: Weber and Morris intra-particle diffusion model for the adsorption of MTB onto MPPB at 303 K and 120 min

3.20 Liquid Film Diffusion Kinetic Model

The contact between MPPB and liquid films of MTB as the rate limiting step was in consideration in simulating the data into equation 12 (Yang et al., 2016; Nworie et al., 2019). The linear form of the equation is shown in Table 2 with Klf as slope which stands for liquid diffusion constant (1/min) and detects sorbate transfer coefficient as controlled by external mass sorption medium.

$$In(1 - \frac{qt}{qe}) = -K_{lf} t \quad (12)$$

From Figure 21, a linearplot of in $(1 - \frac{qt}{qe})$ against t gave R^2 value of 0.5171 which is very low and cannot simulate the data very well. However, the value of the slope as shown in Table 4 indicated presence of liquid diffusion and further supports presence of boundary layer as a rate determining step. Consequently, the Weber and Morris intra-particle diffusion and liquid film diffusion involving boundary layer action implicates mass movement of MTB into the surface pores of PMMB (Nworie and Spectral, 2018).

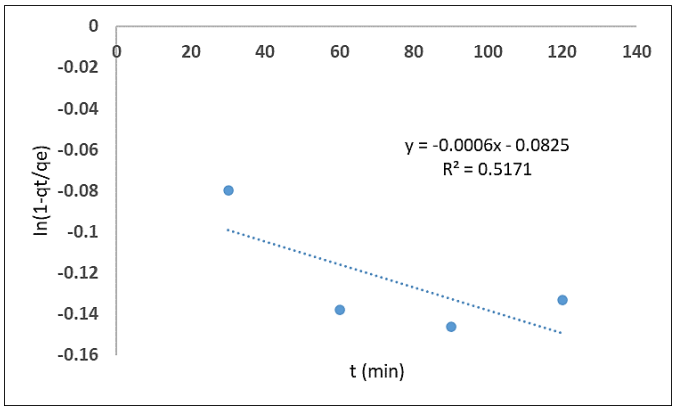

Figure 21: Liquid film diffusion modelfor the adsorption of MTB onto MPPBat 303 K and 120 min

3.21 Bangham's Pore Diffusion Model

The kinetic data was simulated into the Bangham's pore diffusion kinetic model with model equation shown as equation 13 where Co, V, m, Δβ and $K_B$represents initial metal ion concentration (mg/L), volume of solution (mL), weight of adsorbent (g/L), slope and intercept respectivelywith the linearized form in Table 2 (Coskun et al., 2017; Nworie et a., 2019).

$$\text{Log log}\left\{\frac{\text{Co}}{Co - mqt}\right\} = \text{Log}\left\{\frac{\text{m}K_B}{2.303V}\right\} + \delta\beta log t \quad (13)$$

Figure 22 shows the linear plot of log log [Co/Co-mqt] against log t with a very poor R^2 value of 0.0907, an indication of the inability of the model to simulate the kinetic data perfectly well. This implies absence of pore diffusion in the sorption process.

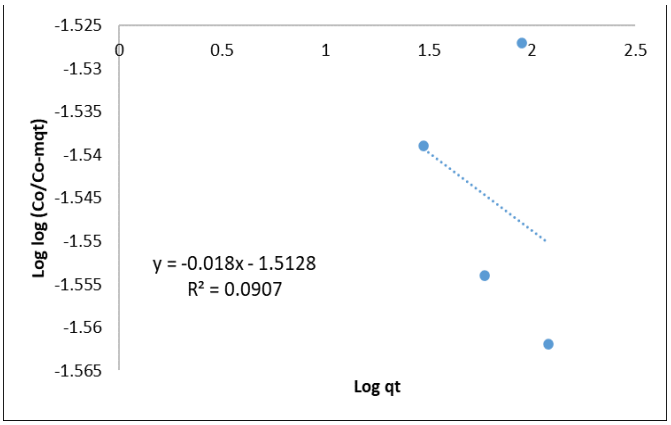

Figure 22: Bangham's pore diffusion model for the adsorption of MTB onto MPPBat 303 K and 120 min

3.2 Mass Transfer Model and Adsorption Diffusion Studies

3.22.1 Mass transfer model

The simulation of the data into mass transfer model which is of high industrial relevance was done. The mass transfer model is shown in equation18and the linear form as shown in Table 2 (Etim et al., 2016).

$$\text{Co} - \text{Ct} = \text{Dexp}(K_o t) \quad (14)$$

From Figure 23, the plot of In (Co-Ct) against t gave R^2 value of 0.9986very close to Elovic model R^2 of 0.9988 with slope and intercept as -34.31 and 3.129 respectively. The R^2 value indicated that the sorption process follows the mass transfer process as supported by weber and Morris and liquid film diffusion kinetic processes. The multifunctional surfaces (many functional groups resulting from modification) of MPPB could have enhanced the mass transfer of MTB as projected in mass transfer processes. Therefore, diffusion of ions from MTBto the surface of MPPB, diffusion of ions within the MPPBand chemical interaction between the ions and the multifunctional groups of the MPPB could likely be the internal and external mechanisms regulating the mass transfer processes in the sorption (Nworie et al., 2020).

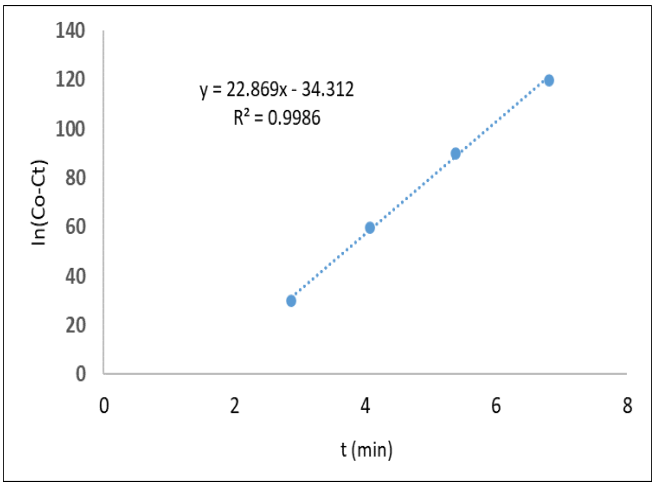

Figure 23: Mass transfer model for the adsorption of MTB onto MPPBat 303 K and 120 min

3.22.2 Dunwald-Wagner Model

The data obtained was simulated into mass transfer model which basically involves intra-particle diffusion process proposed by Dunwald-Wagner and is as shown in equation 15 and the linear form in Table 2 (Akkaya and Guzel, 2014). The plot of t versus Log (1- qt/qe)² is shown in Figure 24 with very low R² value of 0.5034 indicating the inability of the model to simulate the data perfectly well.

$$Log(1-(\frac{qt}{qe})^2) = -K_{DW}t \quad (15)$$

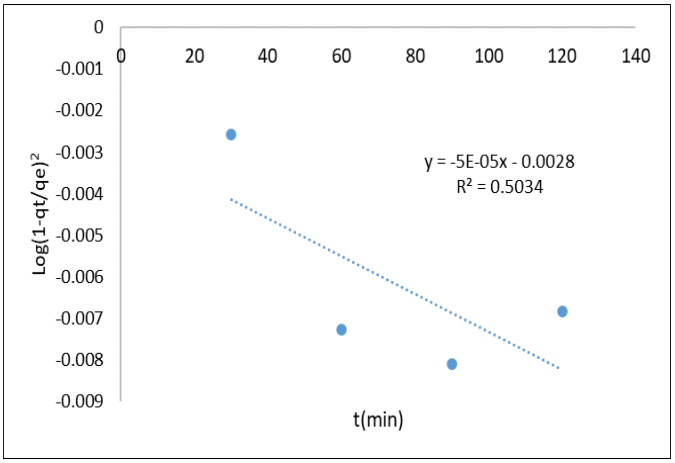

Figure 24: Dunwald wagner model for the adsorption of MTB onto MPPB at 303 K and 120 min

Table 1: Isotherm Models and Their Linear Forms

S/N	Model Type	Models	Linearized Equation	Reference
1	One parameter	Henry	$q_e = KH_E C_e$	(Nworie et al., 2019)
2	Two parameter	Langmuir	$\frac{\mathrm{Ce}}{\mathrm{qe}} = \frac{\mathrm{Ce}}{\mathrm{Qm}} + \frac{1}{\mathrm{bQm}}$	(Halil et al., 2017; Pereira et al., 2009)
3	Two parameter	Freundlich	$\mathrm{In}\frac{q_e}{Ce} = \mathrm{InK}_{Eq_m} - \frac{q_e}{nq_m}$	(Farouq and Yousef, 2015; Oyebado et al., 2004)
4	Two parameter	Elovic	$\mathrm{Inq}_e = \mathrm{InK}f + \frac{1}{n}InCe$	(Nworie et al., 2019)
5	Two parameter	Temkin	$\mathrm{q}_e = \beta\mathrm{InA}_t + \beta InCe$	(Farouq and Yousef, 2015)
6	Two parameter	Jovanovic	$Inq_e = Inq_m - K_f C_e;$	(Farouq and Yousef, 2015)
7	Two parameter	Harkin-Jura	$\frac{1}{q_e^2} = \frac{B}{A} - (\frac{1}{A})logC_e$	(Nworie et al., 2019)
8	Two parameter	Hill	$Log\frac{q_e}{q_H - q_e} = nHlog(C_e) - \log(K_D)$	(Nworie et al., 2019)
9	Three parameter	Redlich-Peterson	$In\left(\frac{C_e}{q_e}\right) = \beta InC_e - InA$	(Nworie et al., 2019)

Table 2: Kinetic Models, Linear Forms and Plots

S/N	Kinetic Models	Linearized Equation Form	Reference
1	Pseudo-First order	$\mathrm{In(qe - qt)} = \mathrm{In}qe - k_1 t$	(Farouq and Yousef, 2015)
2	Pseudo-second order	$\frac{t}{q_t} = \frac{1}{K_2}{q_e}^2 + \frac{t}{q_e}$	(Nworie et al., 2019)
3	Elovic	$\mathrm{q}_t = \frac{1}{\beta}\mathrm{In}(\alpha\beta) + \frac{1}{\beta}In(t)$	(Yang et al., 2016; Nworie et al., 2019)
4	Weber and Morris	$qt = K_I t^{1/2} + C$	(Farouq and Yousef, 2015)
5	Liquid film diffusion	$In(1-\frac{qt}{qe}) = -K_{lf}t$	(Shakoor and Nasar, 2016)
6	Bangham pore diffusion	$\mathrm{Log\,log}\left\{\frac{\mathrm{Co}}{Co - mqt}\right\} = \mathrm{Log}\left\{\frac{\mathrm{m}K_B}{2.303V}\right\} + \delta\beta logt$	(Nworie et al., 2020)
7	Mass transfer model	$\mathrm{Co - Ct} = \mathrm{In\ (Co - Ct)} = K_o t + In\ D$	(Nworie et al., 2020)
8	Dunwald -Wagner model	$Log(1-(\frac{qt}{qe})^2) = -K_{DW}t$	(Nworie et al., 2020)

Table 3: Isotherm Model Constants and Their Error Analysis

S/N	Type of Model	Models	Parameter 1	Parameter 2	Parameter 3	R^2	$1-R^2$
1	One parameter	Henry	KH_E = 87.63			0.9126	0.0874
2	Two parameter	Langmuir	q_m (mg^{-1}) =222	b(Lmg^{-1}) = 0.247		0.9836	0.0164
3	Two parameter	Freundlich	n= 0.029	K_F ($mg^{1-1/n}L^{1/n}g^{-1}$) =8.135		0.9388	0.0612
4	Two parameter	Elovic	K_E (Lmg^{-1}) = 0.378	q_m(mgg^{-1})= 1.96		0.9969	0.0031
5	Two parameter	Temkin	K_T(Lmg^{-1}) = 11.05	B($KJmol^{-1}$)=0.163		0.8679	0.1321
6	Two parameter	Jovanovic	K_J (Lg^{-1})= -0.8093	q_m(mgg^{-1}) = -2.95		0.9682	0.0318
7	Two parameter	Harkin-Jura	A_H(g^2L^{-1}) = -0.0028	B_H(mg^2L^{-1})=0.150		0.4738	0.5262
8	Two parameter	Hill	nH=2.51	K_D= 0.955		1	0.0000
9	Three parameter	Redlich-Peterson	A(Lg^{-1}) = 0.0698	B(Lmg^{-1})=34.22	β=0.99	0.8785	0.1215

Table 4: Kinetic Model Constants and Their Error Analysis

S/N	Kinetic Models	Constant 1	Constant 2	R^2	$1-R^2$
1	Pseudo-First order	q_e = 0.177	K_1=0.01	0.9811	0.0189
2	Pseudo-Second order	q_e= 222.2	K_2 = 0.025	0.9597	0.0403
3	Elovic	α= -6.42	β=2.94	0.9988	0.0012
4	Weber and Morris	C=-0.047	K_2=0.013	0.9891	0.0109
5	Liquid film diffusion	K_{lf}= 0.224	qe= -0.0006	0.5171	0.4829
6	Bangham pore diffusion	Δβ=1.66	Kβ=-1.512	0.0907	0.9093
7	Dunwald-Wagner	qe =8.6	K_{dW} = -0.0028	0.5034	0.4966
8	Mass transfer	D= 3.129	K= -34.31	0.9986	0.0014

Key: K(min^{-1}),q_e(mgg^{-1})= K_2($gmg^{-1}min^{-1}$), K_i($mgg^{-1}min^{-1/2}$),α($mgg^{-1}min^{-1}$),β(gmg^{-1}).

4. Conclusion

In conclusion and based on the result of the study, MPPB was synthesized from a very cost effective, environmentally friendly lignocellulosic waste material for use as a sorbent for the removal of MTB from aqueous solution. The synthesized acid modified nanobiosorbent has high maximum adsorption capacity which compares with other biosorbents and activated carbon. The effect of time of contact, pH and initial metal ion concentration were optimized for the sorption of MTB onto MPPB. The nature of MPPB from BET, XRD, SEM analysis indicated that it is mesoporous, crystalline with enough pores to capture pollutants in solution. Based on the equilibrium data simulated into the various models, it was identified that the adsorption process followed perfectly the Hill isotherm model. Also, kinetic data fits well into the Elovic and mass transfer models implicating chemisorption and inner sphere complexation as the rate determining state. Error analysis of coefficient of non-determination was used to further explain the data and their model fits. The biosorbent is effective, low cost, efficient an environmentally friendly for the removal of MTB pollutants from environmental samples.

References

Akkaya, G., Guzel, F., 2014. Application of some domestic wastes as new low-cost biosorbents for removal of methylene blue: kinetic and equilibrium studies. ChemEngCommun., 201 (4), Pp. 557-578.

ALOthman, Z.A., 2012. A Review: Fundamental Aspects of Silicate Mesoporous Materials. Materials, 5, Pp. 2874-2902.

Antonija, K., Natalija, V., Damir, H., and Davor, K., 2018. Lignocellulosic Materials as Dye Adsorbents: Adsorption of Methylene Blue and Congo Red on Brewer's Spent Grain, Croatia Chemical Acta, 91 (1), Pp. 53-64.

Banerjee, S., Chattopadyaya, M.C., 2017. Adsorption characteristics for the removal of a toxic dye, tartrazine from aqueous solutions by a low-cost agricultural by-product. Arabian Journal of Chemistry, 10, S1629-S1638

Betiku, E., Sheriff, O.A., 2014. Modeling and optimization of Thevetiaperuviana (yellow oleander) oil biodiesel synthetic via Musa paradisiacal (plantain) peels as heterogeneous base catalyst: A case of artificial neural network vs. response surface methodology. Ind. crop. prod., 53, Pp. 314-22.

Coşkun, R., Yıldız, A., Delibaş, A., 2017. Removal of Methylene Blue Using Fast Sucking Adsorbent. JMES, 8 (2), Pp. 398-409.

El-Sayed, G.O., 2011. Removal of Methylene Blue and Crystal Violet from aqueous solutions by palm kernel fiber, Desalination, 272 (3), Pp. 225-232.

Etim, U.J., Umoren, S.A., Eduok, U.M., 2016. Coconut coir dust as a low cost adsorbent for the removal of cationic dye from aqueous solution. Journal of Saudi Chemical Society, 20 (1), Pp. 67-76.

Farouq, R., and Yousef, N.S., 2015. Equilibrium and Kinetics Studies of adsorption of Copper (II) Ions on Natural Biosorbent. International Journal of Chemical Engineering and Applications, 6, Pp. 319 – 324.

Halil, K., Serpil, S., Ramazan, C., and Mutlu, Y., 2017. Adsorption of methylene Blue from Aqueous Solution with Vermicompost Produced Using Banana Peel. International Journal of Modern Engineering Research, 7 (7), Pp. 64-73.

Inyang, M., Cao, B., Pullammannappallil, P., Zimmerman, A.R., 2011. Enhanced lead sorption by biochar derived from anaerobically digested sugarcane bagasse. Sep. Sci. Technol., 46 (12), Pp. 1950-6.

Jianjian, Z., Yuzhong, N., Bing, R., Hou, C., Shengxiao, Z., Jilan, J., Yao, Z., 2018. Synthesis of Schiff base functionalized super paramagnetic Fe304 composites for effective removal of Pb(II) and Cd(II) from aqueous solution. Chemical engineering journal, 347, Pp. 574-584.

Kamal, Amin, N., 2009. Removal of direct blue-106 dye from aqueous solution using new activated carbons developed from pomegranate peel: Adsorption equilibrium and kinetics. Journal Of Hazardous Material, 165 (1-3), Pp. 52-62.

Kezerle, A., Velic, N., Hasenay, Kovacevica, D., 2018. Lignocellulosic materials as adsorbents: Adsorption of MEB and Congo red on brewers spent grain. Croat. Chem. Acta., 91, Pp. 53-64.

Komkiene, J., Baltrenaite, E., 2016. Biochar as adsorbent for removal of heavy metal ions [Cadmium (II), Copper (II), Lead (II), Zinc (II) from aqueous phase. Int. J. Environ. Sci. Technol., 13, Pp. 471-82.

Mahmoodi, N.M., Salehi, R., and Arami, M., 2011. Binary System Dye Removal from coloured Textile Wastewater using activated carbon. Kinetics and Isotherm Studies, Desalination, 3 (1), Pp. 111-122.

Mazhar, I.K., Saima, Q.M., Sajida, P., Muhammed, Y.K., 2014. Citrus paradise: An effective bio-adsorbent for arsenic(V) remediation. Park. J. Anal. Environ. Chem., 15 (1), Pp. 35-41.

Nworie, F., Nwabue, F., Ikelle, L., Ogah A., Elom, N., Iloch, N.O., Itumoh, E.J., Oroke, C.E., 2018. Activated plantain peel biochar as adsorbent for sorption of zinc (II) ions: equilibrium and kinetics studies. JOTCSA, 5 (3), Pp. 1257-1269

Nworie, F.S., 2018. Spectral, Thermal and In Vitro Antibacterial Studies on Cadmium (II)–bis(2,2/-methylidenephenol) diaminoethane. Journal of the Turkish. Chemical Society Section A: Chemistry, 5 (3), Pp. 1029-1036.

Nworie, F.S., Nwabue, F.I., 2017. Synthesis, Optimization, Characterization and Antimicrobial Studies of Cu (II) and Co (III) Complexes of Bis(2,2/-methylylidenephenol) diaminoethane. Chemistry. Journal of Moldova, General, Industrial and Ecological Chemistry, 12 (2), Pp. 41-49

Nworie, F.S., Nwabue, F.I., Oti, W., Mbam, Eand Nwali, B.U., 2019. Removal of Methylene Blue from Aqueous Solution Using Activated Rice Husk Biochar: Adsorption Isotherms, Kinetics and Error Analysis, J.Chil. Chem. Soc., 64, Pp. 4365-4376.

Nworie, F.S., Nwabue, F.I., Oti, W., Omaka, N.O., and Igwe, H., 2020. Hydrothermal Synthesis of Multifunctional Biochar-supported SALEN Nanocomposite for Adsorption of Cd (II) Ions: Function, Mechanism, Equilibrium and Kinetic Studies. Anal. Bioanal. Chem. Res., 8 (1), Pp. 91-112.

Nworie, F.S., Oroke, E.C., Ikelle, I.I. and Nworu, J.S., 2020. Equilibrium and Kinetic Studies for the Adsorptive Removal of Lead (II) Ions from Aqueous Solution Using Activated Plantain Peel Biochar. Acta Chemica Malaysia, 4 (1), Pp. 9-16.

Okareh, O.T., Adeolu, A.T., 2015. Removal of Lead ion from industrial effluent using plantain wastes. Br. J. App. Sci. Technol., 8 (3), Pp. 267-276.

Onyebado, C.O., Iyagba, E.T., Offor, O.J., 2004. Solid soap production using plantain peels ash as source of alkali. Journal of Applied Science and Environmental Management, 6, Pp. 73-7.

Ozdes, D., Gundogdu, A., Duran, C., and Hasan B.S., 2010. Evaluation of adsorption characteristics ofmalachite green onto almond shell (Prunusdulcis) Separation. Science and Technology, (45), Pp. 2076.

Pereira, M.D.G., Korn, M., Santos, B.B., Ramos, M.G., 2009. Vermicompost for Tinted Organic Cationic DyesRetention. Water Air Soil Pollution, 200 (1-4), Pp. 227-235.

Phansiri, M., Wanwimon, P., Sataporn, K., 2015. Characterization and Properties of Activated Carbon Prepared from Tamarind Seeds by KOH Activation for Fe (III) Adsorption from Aqueous Solution, The Scientific World Journal, 8 (2), Pp. 147-156.

Pushpa, T.B., Vijayaraghavan, J., SardharBasha, S.J., Sekaran, V., Vijayaraghavan, K., Jegan, J., 2015. Investigation on removal of malachitegreen using EM based compost as adsorbent. Ecotoxicology and Environmental Safety, (118), Pp. 177-182.

Santos, M.S.F., Schaule, G., Alves, A., Madeira, L.M., 2013. Adsorption of paraquat herbicide on deposits from drinking water Networks. Chem. Eng. J., (229), Pp. 324-333.

Shakoor, S., Nasar, A., 2016. Removal of methylene blue dye from artificially contaminated water using citrus limetta peel waste as a very low-cost adsorbent. Journal of the Taiwan Institute of Chemical Engineers, (66), 154-163.

Tan, I.A.W., Ahmad, A.L., Hameed, B.H., 2008. Adsorption of basic dye on high-surface-area activated carbon prepared from coconut husk: Equilibrium, kinetic and thermodynamic studies. Journal of Hazardous Materials, 154 (1-3), Pp. 337-346.

Tiwari, L.D, Lee, S., 2012. Activated carbon and manganese coated activated carbon precursor to dead biomass in the remediation of arsenic contaminated water. Environmental Engineering Research., 17, Pp. 541-8.

Yang, G., Xian, Q., Shen, F., Wu, J., and Zhang, Y., 2016. Removal of Congo Red and Methylene Blue from aqueous solutions by vermicompost-derived biochars, Plos one, 11 (5), Pp. 1-18.

You, H., Chena, J., Chao Yang, C., Xua, L., 2016. Selective removal of cationic dye from aqueous solution by low-cost adsorbent using phytic acid modified wheat straw. Colloids and Surfaces A: Physicochem. Eng. Aspects, (509), Pp. 91-98.

Zhang, L., Guo, J., Huang, X., Wang, W., Sun, P., Lib, Y., Han, J., Functionalized Biochar-Supported Magnetic MnFe2O4 Nanocomposite for the Removal of Pb (II) and Cd (II). RSC Adv., 9, Pp. 365.